1 **Dynamic path dependent landslide susceptibility modelling**

2 Jalal Samia [1, 2], Arnaud Temme [3, 4], Arnold Bregt [1], Jakob Wallinga [2], Fausto Guzzetti [5], Francesca Ardizzone [5]

3 [1] Laboratory of Geo-Information Science and Remote Sensing, Wageningen University & Research, 6708 PB

4 Wageningen, Droevendaalsesteeg 3, The Netherlands

5 [2] Soil Geography and Landscape group, Wageningen University & Research, 6708 PB, Wageningen,

6 Droevendaalsesteeg 3, The Netherlands

7 [3] Department of Geography, Kansas State University, 920 N17th Street, Manhattan, KS, 66506, United States

8 [4] Institute of Arctic and Alpine Research, University of Colorado, Campus Box 450, Boulder, CO 803309-0450,

9 Colorado, United States

10 [5] Istituto di Ricerca per la Protezione Idrogeologica, Consiglio Nazionale delle Ricerche, via Madonna Alta 126,

11 06128 Perugia, Italy

12 **Correspondence**: Jalal Samia, jalal.samia@wur.nl, +31617699436, +31 (0)317 – 419000

13

14 **Abstract**

15 This contribution tests the added value of including landslide path dependency in statistically-based landslide

16 susceptibility modelling. A conventional pixel-based landslide susceptibility model was compared with a model

17 that includes landslide path dependency, and with a purely path dependent landslide susceptibility model. To

18 quantify path dependency among landslides, we used a Space-Time Clustering (STC) measure derived from

19 Ripley's space-time K function implemented on a point-based multi-temporal landslide inventory from the

20 Collazzone study area in central Italy. We found that the values of STC obey an exponential decay curve with

21 characteristic time scale of 17 years, and characteristic space scale of 60 meters. This exponential space-time decay

22 of the effect of a previous landslide on landslide susceptibility was used as the landslide path dependency

23 component of susceptibility models. We found that the performance of the conventional landslide susceptibility

24 model improved considerably when adding the effect of landslide path dependency. In fact, even the purely path

25 dependent landslide susceptibility model turned out to perform better than the conventional landslide susceptibility

26 model. The conventional plus path dependent and path dependent landslide susceptibility model and their resulted

27 maps are dynamic and change over time unlike conventional landslide susceptibility maps.

28

29 **1. Introduction**

30 Landslide susceptibility modelling calculates the likelihood of landslide occurrence in a certain location (Brabb,

31 1985). The resulting landslide susceptibility maps from landslide susceptibility models indicate where landslides

32 are likely to occur (Guzzetti et al., 2005). These maps are useful in land use planning and insurance, among others.

33 In this context, different methods and techniques have been used for landslide susceptibility modelling.

34   Reichenbach et al. (2018) classified these methods and techniques into five groups: (i) direct geomorphological

35   mapping, (ii) analysis of landslide inventories, (iii) heuristic or index-based approaches, (iv) physically or process-

36   based methods, and (v) statistically-based techniques.

37   Statistically-based landslide susceptibility techniques have been the preferred technique in the modelling of

38   landslide susceptibility (Reichenbach et al., 2018). In statistical landslide susceptibility modelling, empirical

39   quantitative relations are explored between the spatial distribution of landslides and a set of environmental factors

40   (e.g., slope and geology) (Van Westen et al., 2003; Guzzetti et al., 2005). The spatial distribution of historic

41   landslides, documented in landslides inventories, is therefore a crucial input for statistically-based landslide

42   susceptibility modelling (Guzzetti et al., 2012; Van Westen et al., 2008). Direct field mapping, visual interpretation

43   of aerial photographs and other remote sensing images are the main sources for such mapping of landslide

44   inventories (Guzzetti et al., 2012). Landslides in such inventories are stored as points or polygons. Although

45   polygon-based landslide inventories (Ardizzone et al., 2018; Schlögel et al., 2011; Galli et al., 2008) are becoming

46   increasingly available, in many landslide prone regions only less-detailed point-based landslide inventories are

47   collected (Gorum et al., 2011; Sato et al., 2007; Keefer, 2000). Conditioning attributes used in landslide

48   susceptibility modelling are mainly derivatives of digital elevation models (DEMs) along with geological, soil and

49   land use data (Günther et al., 2014; Neuhäuser et al., 2012; Reichenbach et al., 2018). While geology, land use and

50   soil data are not always available in high detail, DEM-derivatives are easily computed and globally available at a

51   range of resolutions. Therefore, the minimum available dataset for landslide susceptibility modelling includes a

52   point-based landslide inventory and a set of DEM-derived conditioning attributes.

53   Traditionally, landslide susceptibility is considered time-invariant: susceptibility of a place to landslide occurrence

54   is constant over time, at least over decadal scales. Recently, we proposed the concept of time-variant landslide

55   susceptibility, where susceptibility changes over time due to the transient effect of previous landslides on future

56   landslide occurrence (Samia et al., 2017b, a). We referred to such a transient effect as "path dependency", a term

57   adopted from complex system theory where it is used to describe the concept that the history of a system specifies

58   the future behaviour of a system through legacy effects (Phillips, 2006). In our study area in Umbria, central Italy

59   (Figure 1), we identified the existence of path dependency among landslides: earlier landslides locally increased

60   the susceptibility for future landslides for about two decades, during which the susceptibility decays exponentially

61   over time (Samia et al., 2017b). We first implemented the effect of this landslide path dependency in landslide

62   susceptibility modelling at the scale of slope units. Such units divide an area into hydrological units bounded by

63   drainage and divide lines (Carrara et al., 1991; Alvioli et al., 2016). We found that the impact of path dependency

64   on landslide susceptibility models at slope-unit scale was limited (Samia et al., 2018). This limited impact of

65   landslide path dependency on model predictions was probably due to the fact that landslide path dependency

66   affects landslide patterns at spatial scales smaller than slope units, and we hypothesized that differences between

67   models were likely to increase when including path dependency at smaller spatial scales.

68   The objective of this work is thus to consider the effect of landslide path dependency in landslide susceptibility

69   modelling at the resolution of 10×10 m pixels. We hypothesize that including landslide path dependency will

70   improve the performance of landslide susceptibility models. We also explore whether a purely path dependent

71   landslide susceptibility model, i.e. based solely on landslide inventory information, can provide a meaningful

72   landslide susceptibility map. We use the unique multi-temporal landslide inventory from the Collazzone study area

73   (Figure 1) (Guzzetti et al., 2006a; Ardizzone et al., 2007; Ardizzone et al., 2013).
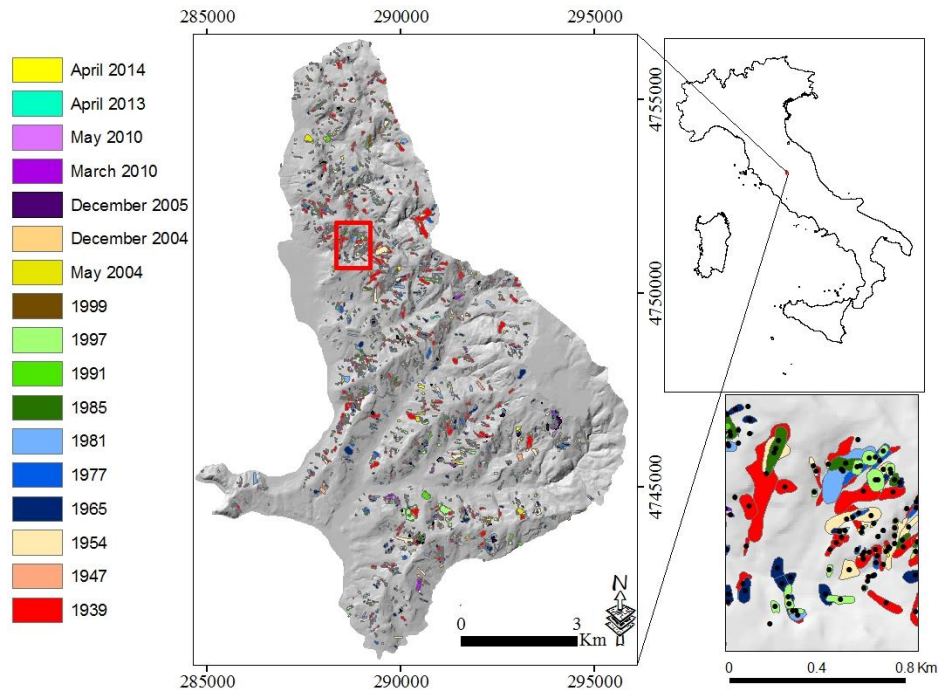
2. Study area and data

75   The Collazzone study area, Umbria, central Italy (Figure 1), extends for about 80 km^2 with terrain elevation

76   between 140 to 632 m and terrain slope derived from a 10×10 m DEM (Figure 2) between 0 to 64°. The DEM

77   was prepared by interpolating 5- and 10-m contour lines shown in 1:10,000 topographic maps (Guzzetti et al.,

78   2006b). A set of DEM-derivatives that has been widely used in landslide susceptibility modelling was computed

79   in SAGA GIS and ArcGIS. We expect that these DEM-derivatives capture topographical, geomorphological and

80   hydrological properties of locations in our study area.

81   The DEM-derivatives (Figure 2) are slope angle, curvature, plan and profile curvature, aspect, northness and

82   eastness as cosine and sine transformations of aspect, topographic position index (TPI) representing different

83   geomorphological settings (Costanzo et al., 2012), stream power index (SPI) representing the erosive power of

84   streams (Moore et al., 1993), topographic wetness index (TWI) as an index for hydrological process in the slope

85   (Jebur et al., 2014). Additionally, for every pixel we computed the distance to the nearest river, the slope length

86   and steepness factor (LS factor) as an index for soil erosion on slope (Moore and Wilson, 1992), the vertical

87   distance to the slope's channel network, and relative slope position representing the relative position of slope in

88   cells between the valley bottom and ridgetop. Additionally, we calculated topographic roughness, which expresses

89   the difference in the values of elevation in the neighbouring cells in the DEM (Riley et al., 1999), and the standard

90   deviation of elevation and slope in a 3×3 pixel window. These 16 DEM-derivatives were used as independent

91   explanatory variables in logistic regression for modelling of landslide susceptibility (see section 3.2).

92   Landslides are abundant in this area, and range from recent shallow landslides to old deep-seated landslides

93   (Guzzetti et al., 2006a). Intense and prolonged rainfall and rapid snowmelt are the main triggers of landslides in

94   the area (Cardinali et al., 2000; Ardizzone et al., 2007). A unique multi-temporal landslide inventory with 3391

95   landslides has been mapped in 19 different time slices. The age of the landslides ranges from relict and very old

96   landslides with an uncertain date of occurrence to landslides that have occurred in 2014. Aerial photographs, direct

97   geomorphological field mapping and satellite images were used for the preparation of the multi-temporal landslide

98   inventory (Ardizzone et al., 2013; Guzzetti et al., 2006a; Galli et al., 2008). Only time slices of the multi-temporal

99   inventory for which the relative date of occurrence is known (Figure 1), were used in this study because time

100   between landslides is a key element in the quantification of landslide path dependency (Samia et al., 2017a, b). In

101   addition, the first time slice, with the known date of 1939, was only used in the computation of the landslide path

102   dependency parameters, and not in landslide susceptibility modelling because of its unknown past. Ultimately, a

103   multi-temporal landslide inventory was used that contains distribution of landslides in16 time slices dating from

104   1947 to 2014 (Figure 1). This multi-temporal landslide inventory was mostly prepared at the scale of 1:10,000

105   which is sufficient for conversion to a 10×10 m pixel-based landslide inventory. However, time slices from 1939

106   to 1997 were prepared from aerial photographs with scales ranging from 1:15,000 to 1:33,000, and this may

107   introduce some positional inaccuracy in landslides, in the order of one pixel. Given that the median size of landslide

108   in this period is 19 pixels, we believe that this is an acceptable level of inaccuracy.

109   More information about the Collazzone study area and the multi-temporal landslide inventory is given in (Galli et

110   al., 2008; Guzzetti et al., 2006a; Guzzetti et al., 2009; Ardizzone et al., 2007).

111

Figure 1. Multi-temporal landslide inventory dating from 1939 to 2014 (left map) (adapted from (Samia et al.,

2018)). Collazzone study area and Umbria region (right upper map). The coordinate system of maps is

EPSG:32633 (www.spatialreference.org). Landslide points were constructed by placing a point in the geometric

centre of each landslide polygon (map in the right lower corner). The red rectangle shows the extent of the map in

the lower right.
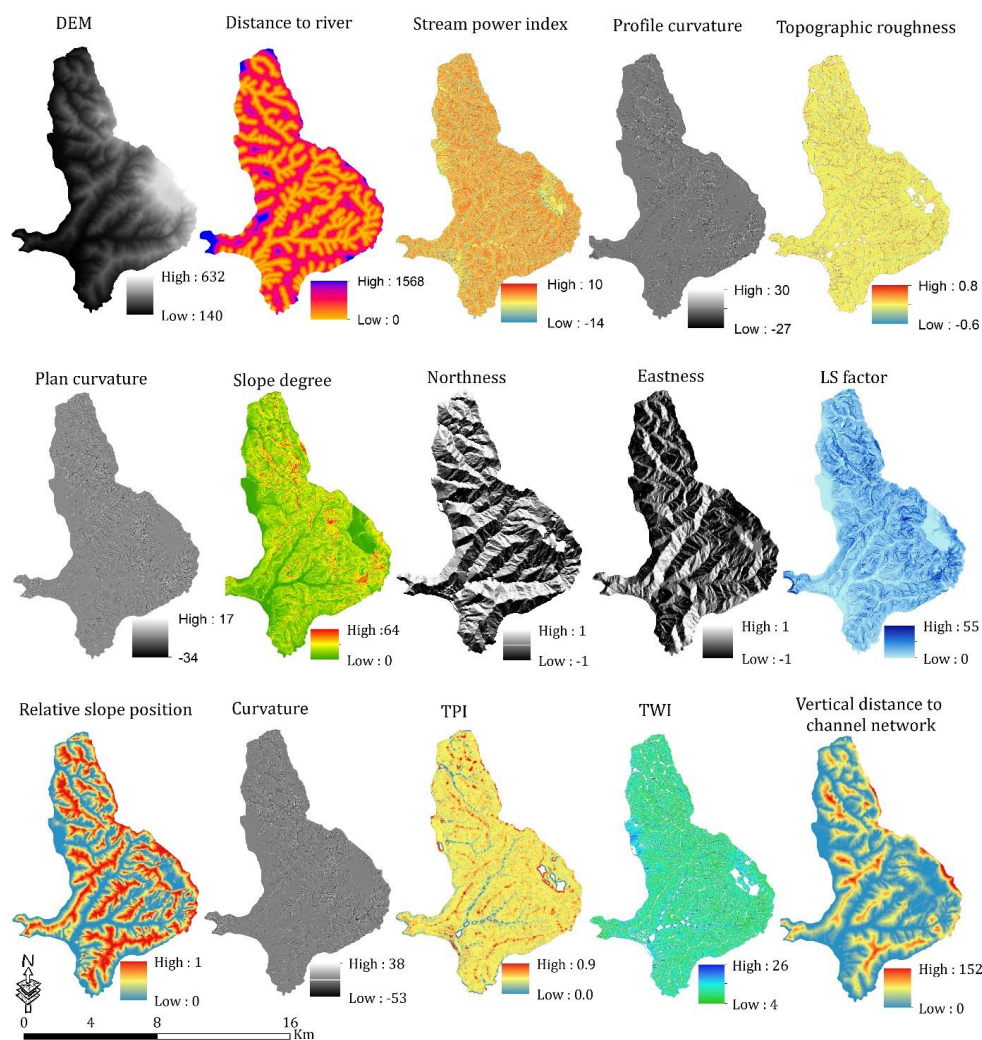
Figure 2. DEM (digital elevation model) and its derivatives used in conventional and conventional plus path dependent landslide susceptibility models. TPI means topographic position index, TWI means topographic wetness index and LS factor stands for slope length and steepness factor.

3. Methods

We used logistic regression to construct three different landslide susceptibility models (Figure 3): (i) a conventional landslide susceptibility model using DEM-derivatives, (ii) a conventional plus path dependent landslide susceptibility model using 16 DEM-derivatives and two landslide path dependency variables (explained below), and (iii) a purely path dependent landslide susceptibility model using only the two landslide path dependency variables. We compared the performance of these models using Area Under Curve (AUC) values from the Receiver Operating Characteristic (ROC) (Mason and Graham, 2002), and selected the optimal model using

128 the Akaike Information Criterion (AIC) (Akaike, 1998), which penalizes the use of additional variables in a model.

129 Ultimately, the coefficients of the variables selected by three landslide susceptibility models and the resulting

130 landslide susceptibility maps were compared.
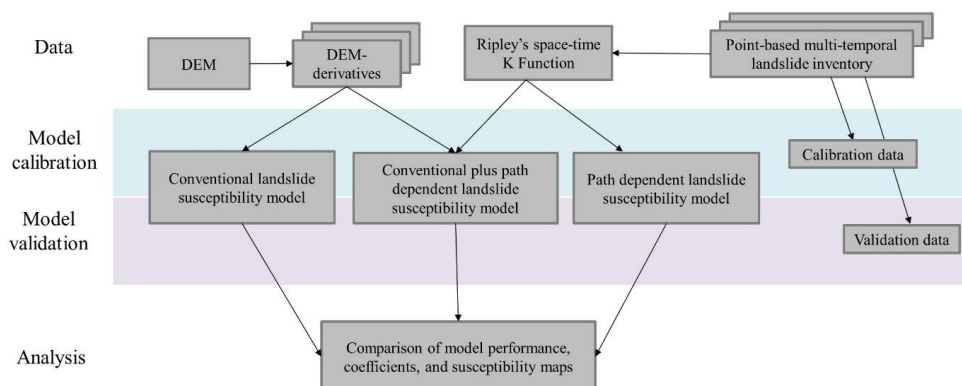
131 **Figure 3.** Flowchart of methods

132

133 **3.1 Quantifying landslide path dependency using Ripley's space-time K function**

134 The spatial-temporal dynamics of landslide path dependency was recently quantified for the Collazzone study area

135 (Samia et al., 2017a), and was implemented in landslide susceptibility modelling at the scale of slope units (Samia

136 et al., 2018). Our previous quantification of landslide path dependency used simplified information about the

137 spatial overlap among landslides in a polygon-based multi-temporal landslide inventory (Samia et al., 2017b). The

138 novel aspect of the present paper is that now, at finer spatial resolution, we quantify landslide path dependency

139 simultaneously in space and time. For this quantification, we use Ripley's K function (Ripley, 1976; Diggle et al.,

140 1995). Ripley's K function has been used mainly in spatial point pattern analysis and reflects the degree of spatial

141 clustering of events (e.g., landslides (Tonini et al., 2014), forest fire (Gavin et al., 2006), crimes (Levine, 2006)

142 and disease outbreaks (Hinman et al., 2006)). The function determines whether events are clustered, dispersed or

143 randomly distributed. A modified Ripley's K function was also used to quantify the degree of clustering of point

144 events in space and time (Lynch and Moorcroft, 2008; Ye et al., 2015). In the landslide path dependency context,

145 we used Ripley's space-time K function to reflect the degree to which landslides occur near previous landslides,

146 and how this changes with increasing distance to the previous landslide in space and time. The starting point to

147 derive Ripley's K is a point-based multi-temporal landslide inventory consisting of points in the geometric centre

148 of polygons of landslides (Figure 1).

149 Ripley's space-time K function tests whether the number of events that is observed in a space-time cylinder around

150 an initial event is equal to what is expected given the average point density in space and time (Ripley, 1976, 1977;

151 Diggle et al., 1995). The space-time cylinder $I_{(h, \Delta)}$ (Figure 4) is defined as:

152 $$I_{(h,\Delta)} \left(d_{ij}, t_{ij} \right) = \begin{cases} 1, \left(d_{ij} \leq h \text{ and } \left(t_{ij} \leq \Delta \right) \right) \\ 0, otherwise \end{cases} \quad (1)$$

153   where h shows the spatial distance increment, Δ shows the time increment, i and j are two landslide centre points,

154   and d and t reflect the distance and time between the two landslide centre points, respectively.
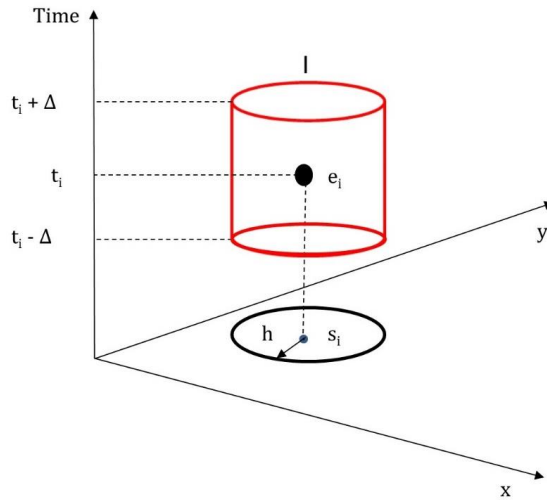
155   **Figure 4.** Space-time cylinder neighbourhood (Smith, 2016) for a landslide event (e_i)

156   The expected Ripley's K function for one space-time cylinder of size h and Δ is defined as:

157     $K(h,\Delta) = \frac{1}{\lambda_{st}} \sum_{j \neq i} E\big[I_{(h,\Delta)} (d_{ij}, t_{ij})\big]$ (2)

158   where E is the expected number of landslides in the cylinder, and λ_{st} reflects the average space-time intensity of

159   the landslides i.e., the expected number of landslides per unit of space-time volume, which is calculated as:

160     $\lambda_{st} = \frac{n}{a(R) \times (t_{max} - t_{min})}$ (3)

161   where n is the number of landslides in the entire inventory, t is time, and $a(R)$ reflects the size of the area. Therefore,

162   the expected Ripley's space-time K function for the space-time cylinders around each landslide point is defined

163   as:

164     $K(h,\Delta) = \frac{1}{n.\lambda_{st}} \sum_{i=1}^{n} \sum_{j \neq i} E\big[I_{(h,\Delta)} (d_{ij}, t_{ij})\big]$ (4)

165   Similarly, the observed Ripley's space-time K function is calculated from the landslide inventory as:

166     $\widehat{K}(h,\Delta) = \frac{1}{n.\widehat{\lambda}_{st}} \sum_{i=1}^{n} \sum_{j \neq i} I_{(h,\Delta)} (d_{ij}, t_{ij}).$ (5)

167   Finally, we defined the space-time clustering (STC) measure, which reflects how much more likely it is that a

168   landslide will occur given a time and space distance from a previous landslide, as following:

169   Empirical $STC(h,\Delta) = \frac{\widehat{K}(h,\Delta)}{K(h,\Delta)}$ -1   (6)

170 STC values > 0 indicate clustering and values < 0 indicate dispersion. We calculated STC (h, Δ) for a wide range

171 of *h* and Δ: values of h ranged from 0 to 500 meter in 30 steps, and values of Δ ranged from 0 to 38 years in 30

172 steps. This yielded 900 empirical values of STC (h, Δ). We then fitted an exponential decay function of *h* and Δ to

173 the empirical STC values. This exponential decay function was used to calculate STC values for each pixel

174 depending on when and where a landslide last occurred closely to that pixel.

175 Based on this, we calculated two landslide path dependency variables. The first variable reflects the maximum

176 value of all STC values for all previous landslides near a pixel. This variable results in high values when one

177 particular previous nearby landslide is expected to have a large impact on the susceptibility of landsliding. The

178 second variable is the sum of all STC values of all previous landslides near a pixel. This variable results in high

179 values when all previous nearby landslides are expected to have a large impact on the susceptibility of landsliding.

180 This approach mirrors what we did in our slope unit-based susceptibility model (Samia et al., 2018) in the sense

181 that the variables separate the impact of the most impactful previous nearby landslide from the impacts of all

182 previous nearby landslides.
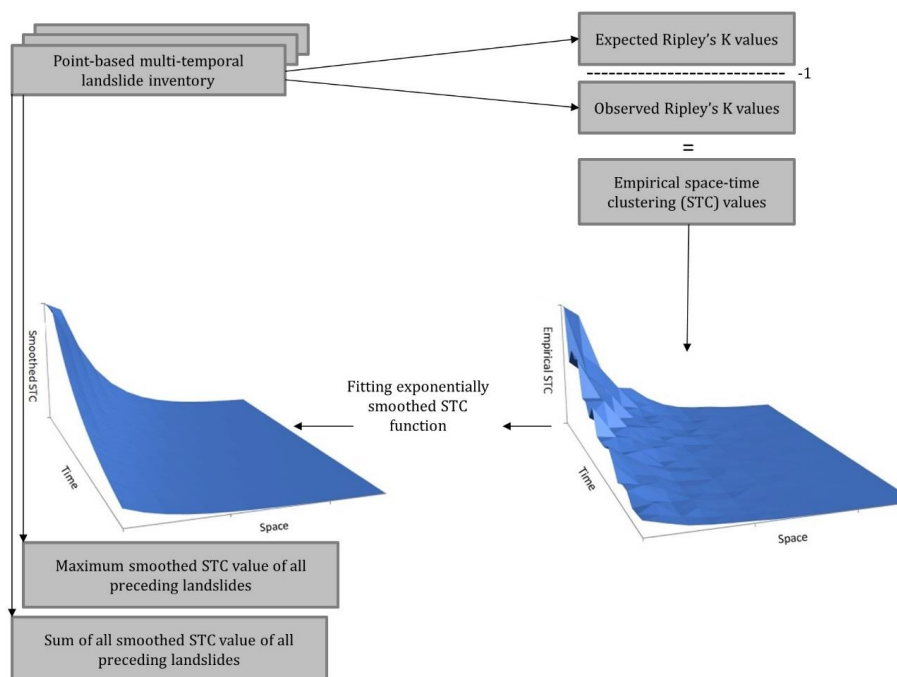
183 **Figure 5.** Procedure to compute the two landslide path dependency variables using Ripley's space-time K function.

184 **3.2 Logistic regression**

185 Logistic regression is considered a reference model in statistically-based landslide susceptibility modelling

186 (Reichenbach et al., 2018). Relations between presence and absence of landslides as a binary target variable are

187 explained by a set of independent variables such as slope steepness and slope position in logistic regression. In

Natural Hazards
and Earth System
Sciences
Discussions

188   this paper, DEM-derivatives (section 2 and Figure 2) as well as the two landslide path dependency variables

189   computed using the Ripley's space-time K function (see section 3.1) were used as independent variables. Landslide

190   presence or absence was the binary target variable.

191   **3.3 Training and testing**

192   When using a multi-temporal landslide inventory in landslide susceptibility modelling, the selection of time slices

193   for the training and testing is crucial. In Rossi et al. (2010) and Samia et al. (2018), a sequential splitting sampling

194   strategy was used in such a way that landslides in older time slices were used to train the model and landslides in

195   newer time slices were used to test the model. However, such a sequential sampling strategy does not provide an

196   equal range of landslide histories between training and testing datasets and this could bias the role of time in path

197   dependent landslide susceptibility modelling. To avoid such a timing inequality, Samia et al. (2018) also

198   introduced a non-sequential sampling strategy in which the span of timing segregation among time slices in the

199   training and the testing datasets is comparable. In this study, we used this sampling strategy to split the multi-

200   temporal landslide inventory into training and testing datasets. To achieve this, landslides in the time slices of

201   1947, 1954, 1981, 1985, 1999, May 2004, March and May 2010 were used for training, and landslides in the time

202   slices of 1965, 1977, 1991, 1997, December 2004 and 2005 and April 2013 and 2014 were used for testing (Figure

203   1). It is important to note that the time slice in 1939 was used only for quantification of landsliding history of the

204   other time slices, and not for training or testing. Thus, the 1st time slice in the training dataset is 1947 (Figure 1).

205   The number of pixels with landslides was smaller than the number of pixels without landslides in both training

206   and testing datasets. Therefore, we randomly selected 5,000 pixels with landslides and 5,000 pixels without

207   landslides to create equal datasets for training and testing. This random selection of pixels was repeated 10 times

208   both in the training and testing datasets. After preparation of the 10 training datasets, logistic regression was

209   applied to the10 training datasets with entry probability of 0.05 and removal probability of 0.06 for independent

210   variables to diminish the chance of overfitting in the model. We only allowed inter-variable correlations less than

211   0.8 to avoid multicollinearity. Model performance was assessed using AUC and AIC values. The AUC values for

212   testing were assessed using 10 training models and 10 independent testing datasets. The models with highest

213   performance in terms of AUC values, were used to map susceptibility to landslides. Finally, we compared landslide

214   susceptibility maps resulting from conventional, conventional plus path dependent and purely path dependent

215   susceptibility.

216   **4. Results**

217   **4.1 Spatial-temporal dynamic of landslide path dependency**

218   Ripley's space-time K function confirmed the existence of landslide path dependency at small spatial and small

219   temporal distances from a previous landslide (Figure 6). The STC measure (Eq 6) is high in the space-time vicinity

220   of an earlier landslide, and it then decreases rapidly. Apparently, landslide susceptibility is relatively high

221   immediately after occurrence of an earlier, nearby landslide.

222

223

224
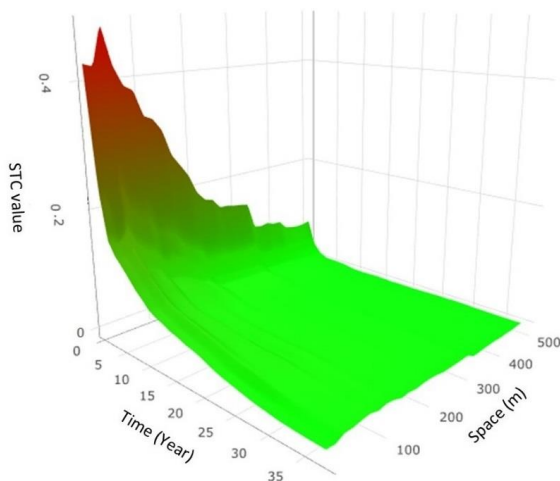
Figure 6. Space-time dynamic of landslide path dependency.

226 The exponential decay function that was fitted to the empirical STC values is:

227 $$Smoothed\ STC(t,d) = 0.44 * e^{(-t/16.7)} * e^{(-d/58.8)} \qquad (7)$$

228 This function shows that the STC measure decays exponentially over a characteristic time scale of 16.7 years and

229 characteristic spatial scale of 58.8 meters. The residual standard error of the exponential function is 0.01, in units

230 of STC (-), which compares favourably with the actual values that range up to 0.44.

231 **4.2 Model performance**

232 We compared performance of the conventional, conventional plus path dependent, and purely path dependent

233 landslide susceptibility models, using AUC (greater is better) and AIC (lower is better) values as measure of

234 performance. The best performing landslide susceptibility model was the conventional plus path dependent model,

235 both when expressed as AUC values and as AIC values (Table 1). The purely path dependent landslide

236 susceptibility model, constructed with only the two landslide path dependency variables, performed better than the

237 conventional landslide susceptibility model with its 16 DEM-derived variables.

238 **Table 1.** Performance of the three landslide susceptibility models

AUC and AIC values	Conventional susceptibility model	Conventional plus path dependent susceptibility model	Path dependent susceptibility model
AUC training	0.704 ± 0.006	0.764 ± 0.003	0.721 ± 0.004
AIC training	$12,678 \pm 82$	$11,711 \pm 53$	$12,469 \pm 62$
AUC testing	0.682 ± 0.007	0.732 ± 0.004	0.698 ± 0.004

239

240 For conventional susceptibility models, 6 DEM-derivatives were selected in all 10 models (Table 2). Adding two

241 landslide path dependency variables into DEM-derivatives variables affected the inclusion and exclusion of DEM-

Natural Hazards
and Earth System
Sciences

Discussions

242 derivative variables only slightly. For example, the variables TPI and distance to river were selected 4 and 7 times

243 respectively in the conventional susceptibility models whereas after adding the two landslide path dependency

244 variables, these variables were selected 5 and 4 times respectively. The variable eastness which was selected twice

245 in the conventional susceptibility models, was never selected in the conventional plus path dependent susceptibility

246 models.

247 **Table 2.** Selection of independent variables in conventional, conventional plus path dependent and purely path

248 dependent landslide susceptibility modelling. Variables selected 6 or more times are shown. The numbers between

249 parentheses indicate how often variables were selected.

Three landslide susceptibility models	Number of variables selection in 10 times repetition	Average number of variables selected in the three susceptibility models
Conventional (16 DEM-derivatives)	Elevation (10), standard deviation of slope (10), LS factor (10), standard deviation of elevation (10), stream power index (10), aspect (10), distance to river (7), vertical distance to channel network (6), relative slope position (6)	8.7
Conventional plus path dependent (16 DEM-derivatives plus two landslide path dependency variables)	Elevation (10), standard deviation of slope (10), LS factor (10), standard deviation of elevation (10), stream power index (10), aspect (10), max smoothed STC value (10), sum of all smoothed STC value (10)	10.4
Path dependent (two landslide path dependency variables)	max smoothed STC value (10), sum of all smoothed STC value (10)	2

250

251 In all the training and the testing datasets, the contingency tables (Table 3) showed that conventional landslide

252 susceptibility models differed substantially from the conventional plus path dependent and path dependent

253 landslide susceptibility models. In particular, the percentage of false positives (the percentage of pixels without

254 landslides predicted with landslides) for the conventional susceptibility models is higher than for the two other

255 susceptibility models. However, there are also fewer true negatives (the percentage of pixels without landslides

256 predicted without landslides) in the conventional than in the conventional plus path dependent and path dependent

257 susceptibility models. The variation in the differences is larger in the training datasets than the testing datasets,

258 suggesting that all fitted models are robust.

259

260

261

262

Table 3. Contingency tables computed with cut off value of 0.5 for the three models.

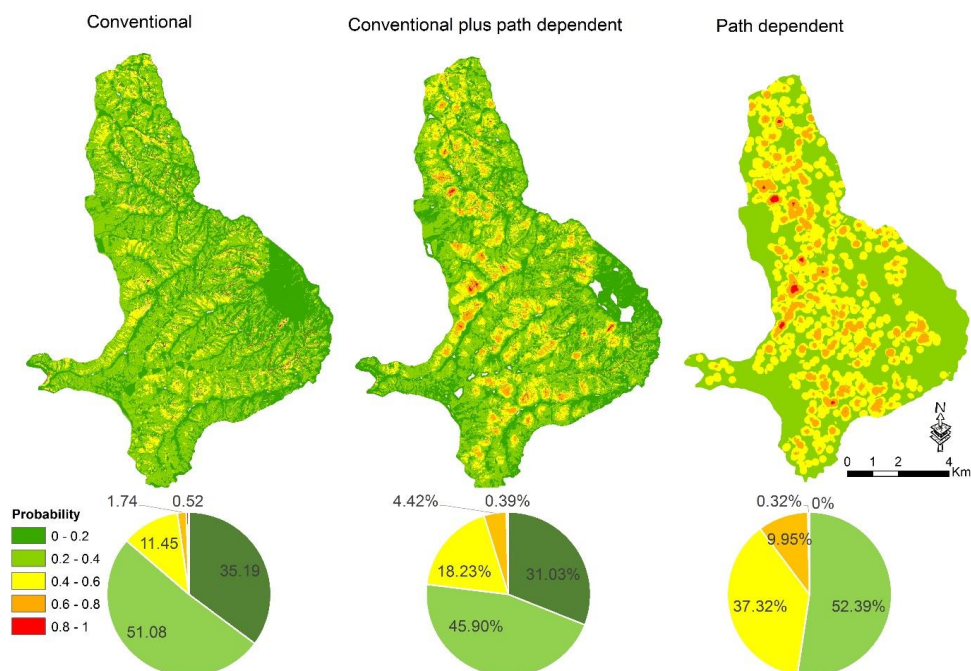|		Conventional landslide susceptibility		Conventional plus path dependent landslide susceptibility		Path dependent landslide susceptibility	
		Observed landslides		Observed landslides		Observed landslides	
		yes	no	yes	no	yes	no
Predicted landslides (training)	yes	35 ± 0.33	19 ± 0.60	34 ± 0.42	14 ± 0.23	31 ± 0.8	13 ± 0.32
	no	15 ± 0.33	31 ± 0.60	16 ± 0.42	36 ± 0.23	19 ± 0.8	37 ± 0.32
Predicted landslides (testing)	yes	33 ± 0.50	19 ± 0.21	29 ± 0.35	13 ± 0.43	23 ± 0.24	12 ± 0.41
	no	17 ± 0.50	31 ± 0.21	21 ± 0.35	37 ± 0.43	27 ± 0.24	38 ± 0.41

264

3.3 Conventional, conventional plus path dependent and purely path dependent landslide susceptibility maps

The landslide susceptibility maps derived from the three models illustrate different patterns of landslide susceptibility (Figure 7). For the models that include path dependency, the presented maps give the average values of all simulated time slices. Differences between the maps correspond with the considerable differences in the performance of their landslide susceptibility models in terms of AUC and AIC values (Table 1). The path dependent landslide susceptibility map is visually different from both other landslide susceptibility maps, with the pattern dominated by regions of high susceptibility around locations where landslides previously occurred.

273

274

Natural Hazards
and Earth System
Sciences
Discussions
Open Access
EGU

Figure 7. Conventional landslide susceptibility map in the left, the conventional plus path dependent landslide susceptibility map (averaged out over 16 time slices) in the middle and path dependent landslide susceptibility map (averaged out over 16 time slices) in the right. The pie charts show the percentage of pixels in each map in different probability levels of landslide occurrence.

The 16 conventional plus path dependent landslide susceptibility maps are dynamic and change over time (Figure 8). These changes reflect the exponential decay with increasing time since previous nearby landslides (Figure 6) and the sudden increase of susceptibility in areas close to recent landslides. The gradual decrease in susceptibility levels is clearest when comparing the 1981 and 2004 susceptibility maps, whereas the sudden increase is clearest when comparing the 2004 and 2014 maps. The 2014 susceptibility map has higher susceptibility levels because of the impact of recent landslides in the year 2013.
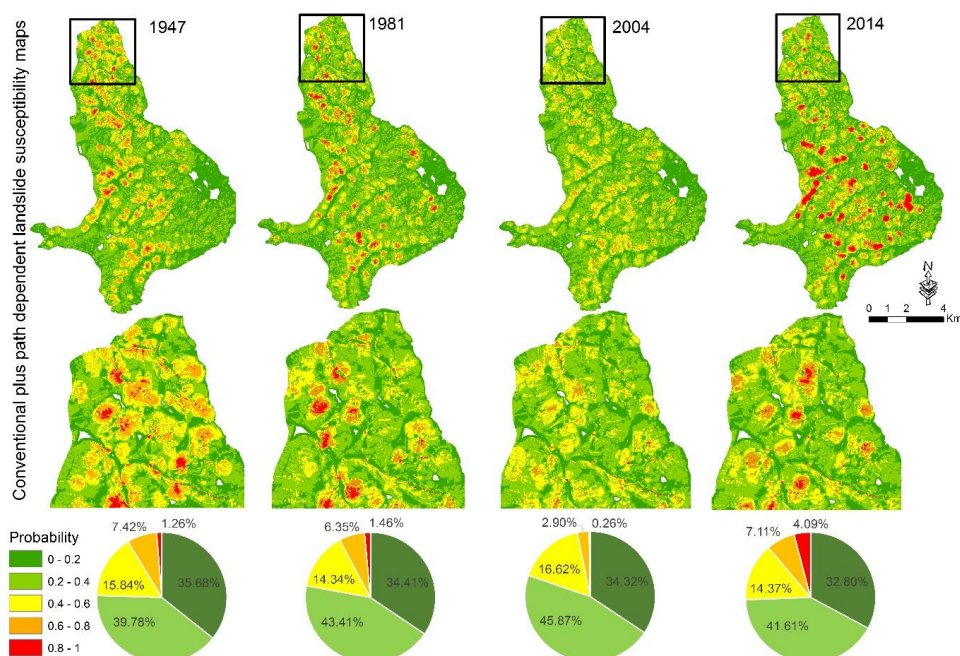
Figure 8. Examples of four dynamic conventional plus path dependent landslide susceptibility maps in the years of 1947, 1981, 2004 and 2014. Zoomed maps show the places where there are large changes in susceptibility over time.

Similar dynamics are visible when comparing landslide susceptibility maps constructed with the purely path dependent model for different years (Figure 9). These maps show only the pure influence of earlier landslides on susceptibility to future landslides (Figure 6). Again, the susceptibility of landslides decreases where distance from earlier landslides in space and time increases, but jumps back up when more recent landslides become part of the landslide history. The pure influence of each individual landslide on the susceptibility to the future landslide is strong when a landslide is fresh which is reflected in the high percentage of susceptibility levels of 0.6-0.8 and 0.8-1.0 in 1947 and 2014.When time passes since the previous landslide has occurred, the susceptibility decreases with an exponential decay response which is reflected in the low percentage of susceptibility levels of 0.6-0.8 and 0.8-1.0 in 1981 and 2004.
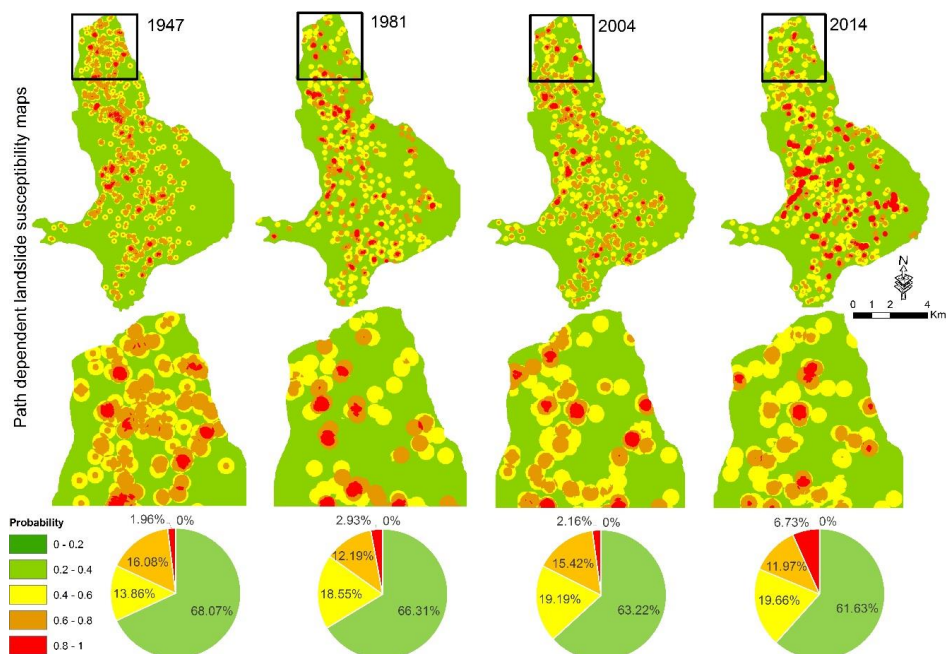
Figure 9. Examples of four dynamic path dependent landslide susceptibility maps in the years of 1947, 1981, 2004 and 2014. Zoomed maps show the places where there are large changes in susceptibility over time.

5. Discussion

In this section, we focus first on the quantification of landslide path dependency in the pixel-based multi-temporal landslide inventory, and then discuss its role in susceptibility models. We also discuss the susceptibility model performance for all three model types. At the end, the exportability of landslide path dependency parameters and the implication of dynamic time-variant path dependent landslide susceptibility in landslide hazard is discussed.

5.1 Quantification of landslide path dependency

The quantification of landslide path dependency using Ripley's space-time K function (Ripley, 1976; Diggle et al., 1995) indicates, in our study area, an exponential decay response in the STC values (Figure 6). This means that there is a positive influence of earlier nearby landslides on susceptibility that decays exponentially in time and space with a characteristic time scale of about 17 years, and a characteristic space scale of about 60 meters. This is in accordance with our previously quantified landslide path dependency using follow-up landslide fraction in which the decay period of landslide path dependency was found to be about two decades (Samia et al., 2017b). Landslide clustering manifests in the form of spatial association among landslides where follow-up landslides occur immediately after and close to a previous landslide (Samia et al., 2017a). Samia et al. (2017b) discussed the possible mechanism in the formation of clusters of landslides in which the size of the initial landslide and changes in hydrology of slope destabilized by a landslide could facilitate the occurrence of follow-up landslides and hence clusters of landslides.

317 STC values and their exponential decay to some extent depend on the method that we have chosen to determine

318 the centre point of landslides when converting polygons of landslides to points of landslides. Our approach was to

319 take the geometric centre, but other options exist (Haines, 1994) and their impact should be explored. Also, in the

320 computation of STC values with Ripley's space-time K function, distance between landslides was calculated using

321 the Pythagorean theorem without distinguishing between distances in the x and y direction. Also we did not include

322 differences in the elevation of centre points in our distance calculations. For future work, it could be interesting to

323 define one dimension as the distance along the slope in the downslope direction and another dimension as the

324 distance in the slope parallel direction, and keeping these two spatial dimensions separate in addition to the

325 temporal dimension.

326 **5.2 Effect of landslide path dependency on performance of landslide susceptibility models**

327 Our results demonstrated that including landslide path dependency effect in a pixel-based landslide susceptibility

328 model constructed by DEM-derivatives improves model performance substantially. This is in line with high AUC

329 and low AIC values for the conventional plus path dependent landslide susceptibility model (Table 1). This

330 confirms our main hypothesis that adding the effect of landslide path dependency boosts the performance of

331 landslide susceptibility models, and is in accordance with our previous expectations regarding stronger effect of

332 landslide path dependency in a pixel-based landslide susceptibility model than in a slope unit-based landslide

333 susceptibility model (Samia et al., 2018). Landslide path dependency is a local effect (apparently with

334 characteristic space scale of about 60 meters) in which an earlier landslide increases the likelihood of follow-up

335 landslide occurrence. Such a local effect is obviously more visible at pixel resolution of 10 m rather than at slope

336 unit resolution (with a median size of 51486 m^2 in our study area).

337 Strikingly, the purely path dependent landslide susceptibility model constructed with only the two landslide path

338 dependency variables performs better than the conventional landslide susceptibility model made by DEM-

339 derivative variables (Table 1). This is potentially interesting since this implies that the landslide inventory itself

340 can be used to map susceptibility to landslide without using DEM-derivatives which have been conventionally

341 used in landslide susceptibility modelling (Varnes, 1984; Guzzetti et al., 2005).

342 Another important aspect of considering landslide path dependency effect in landslide susceptibility modelling is

343 providing dynamic landslide susceptibility maps. Landslide susceptibility maps are usually classified into five

344 levels of probability to landslide occurrence ranging from 0 to 1. In the conventional landslide susceptibility map

345 (Figure 7, right map), the five probability levels of susceptibility by definition remain constant over time since the

346 DEM-derivatives in the model are constant (although DEM-derivatives also change when a landslide occurs, but

347 DEMs are not updated frequently enough to reflect this). In reality, susceptibility maps created with this time-

348 insensitive method are used in planning only for an amount of time roughly equal to the temporal length of the

349 original landslide inventory.

350 However, adding landslide path dependency in landslide susceptibility models, provides dynamic landslide

351 susceptibility maps (Figures 8 and 9) in which the levels of susceptibility change over time, reflecting the

352 exponential decay response of landslide path dependency (Figure 6). The changes are in the places where

353 landslides have already occurred, mainly in probability levels of susceptibility ranging from 0.6 to 1.0. This

354 suggests that the part of area located in the high probability level of susceptibility could switch to the low

355 probability level of susceptibility (0 to 0.6) after a decade. This is exemplified between 1947 and 1954 landslide

356 susceptibility maps, in which about 9 km^2 of study area drops more than 0.1 in their probability of landslide

357 occurrence. After adding the two path dependency variables in the conventional landslide susceptibility modelled

358 with DEM-derivatives, it turns out that the coefficients of all DEM-derivative variables become lower (e.g., LS

359 factor becomes less important).

5.3 Can landslide path dependency parameters be transported to other areas?

361 In landslide prone areas where landslides are documented and mapped in the form of polygon-based multi-

362 temporal inventories, the landslide path dependency can be quantified based on geographical overlap among

363 landslides, and hence used in landslide susceptibility modelling (Samia et al., 2017b; Samia et al., 2018). However,

364 polygon-based multi-temporal landslide inventories are rare to the best of our knowledge, and hence in many areas

365 geographical overlap among landslides cannot be computed. In this paper, we proposed using Ripley's space-time

366 K function to compute landslide path dependency where point-based multi-temporal landslide inventories are used.

367 Using such inventories, our STC measure (Eq. 6) can be used to quantify path dependency among landslides.

368 It is attractive to think that the STC measure (Eq. 6) and its parameters (Eq. 7) can be directly exported to landslide

369 prone areas with substantial geological and topographical similarities. However, to gain confidence in this

370 approach, multi-temporal landslide inventories from such places (e.g., (Schlögel et al., 2011)) need to be

371 interrogated to find out whether path dependency occurs, whether it occurs over similar space and time scales, and

372 whether it adds value to susceptibility modelling. This would also allow us to start exploring what determines the

373 characteristic space and time scales.

5.4 Implications of path dependent landslide susceptibility in landslide hazard assessment

375 We have already modified the definition of conventional landslide susceptibility modelling (Varnes, 1984;

376 Guzzetti et al., 2005) using spatial temporal dynamics of landslide path dependency (Samia et al., 2017a, b) as

377 following:

378 $Landslide\ susceptibility_{s,t} = f\big(conditioning\ attributes_s, landslide\ path\ dependency_{s,t}\big)$ (8)

379 In this study, both conventional plus path dependent and path dependent landslide susceptibility models turned out

380 to perform better than a conventional landslide susceptibility model (Table 1). In both models, availability of a

381 space-time component – reflecting the exponential decay of landslide path dependency – indicates that landslide

382 susceptibility is dynamic. This challenges the way landslide hazard is assessed as landslide susceptibility is an

383 important element of landslide hazard.

384 In landslide hazard assessment, landslide susceptibility as a proxy of 'where landslides occur' is combined with

385 the temporal probability of landslide triggers (mainly rainfall) to determine 'when landslides occur' (Guzzetti et

386 al., 2006a). In this context, a dynamic landslide susceptibility (Eq. 8) needs to be considered in combination with

387 the temporal information of landslide triggers in the assessment of landslide hazard. When substantial landsliding

388 happens during a rainfall event, susceptibility in and around such landslides can be raised for a few decades in

389 which moderate rainfall events may already cause substantial landsliding, which raises susceptibility levels again.

390 (Figure 10). If no substantial triggering event happens over the characteristic time scale of roughly 17 years, the

Natural Hazards
and Earth System
Sciences
Open Access
Discussions
EGU

391 increased susceptibility will be substantially reduced, and a later rainfall event may have less influence on

392 landsliding; the probability of experiencing a follow-up landslide will have decreased.
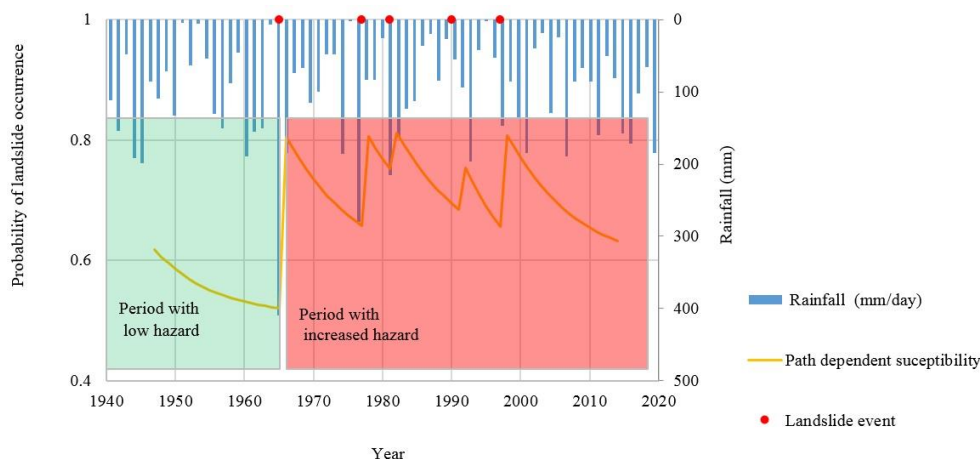
393 **Figure 10.** Hypothetical example of the implication of dynamic path dependent landslide susceptibility model in

394 landslide hazard assessment. When susceptibility is low, the hazard is also low (providing the other components

395 of landslide hazard e.g., size remain unchanged) and large rainfall events are needed to trigger new landslides.

396 Then, when susceptibility is raised by such landslides, the hazard is also high and small rainfall events may trigger

397 new landslides.

398 6. **Conclusion**

399 In the Collazzone study area, in Central Italy, quantification of landslide path dependency reveals an exponential

400 decay response in landslide susceptibility as a function of space and time distance to earlier nearby landslides. For

401 our study area, the characteristic time scale of this effect is about 17 years and the characteristic space scale is

402 about 60 meters. Adding such an exponential decay response of landslide path dependency in conventional pixel-

403 based landslide susceptibility modelled by DEM-derivative improves the performance of model substantially.

404 Taking into account landslide path dependency effects in landslide susceptibility results in dynamic landslide

405 susceptibility models where susceptibility changes over time. We stress that landslide susceptibility modelling

406 should take the effect of landslide path dependency into account since it provides an estimation of temporal

407 validation of different probability levels of landslide occurrence in landslide susceptibility map. The obtained

408 landslide path dependency parameters can possibly be used for dynamic landslide susceptibility modelling in

409 landslide prone areas with environmental and data similarities. We proposed a conceptual model that considers

410 the impact of dynamic path dependent landslide susceptibility on landslide hazard.

411 **Acknowledgement**

416

References

418 Akaike, H.: Information theory and an extension of the maximum likelihood principle, in: Selected Papers of
419 Hirotugu Akaike, Springer, 199-213, 1998.
420 Alvioli, M., Marchesini, I., Reichenbach, P., Rossi, M., Ardizzone, F., Fiorucci, F., and Guzzetti, F.: Automatic
421 delineation of geomorphological slope units with r.slopeunits v1.0 and their optimization for landslide
422 susceptibility modeling, Geosci. Model Dev., 9, 3975-3991, 10.5194/gmd-9-3975-2016, 2016.
423 Ardizzone, F., Cardinali, M., Galli, M., Guzzetti, F., and Reichenbach, P.: Identification and mapping of recent
424 rainfall-induced landslides using elevation data collected by airborne Lidar, Natural Hazards and Earth System
425 Science, 7, 637-650, 2007.
426 Ardizzone, F., Fiorucci, F., Santangelo, M., Cardinali, M., Mondini, A. C., Rossi, M., Reichenbach, P., and
427 Guzzetti, F.: Very-high resolution stereoscopic satellite images for landslide mapping, in: Landslide science and
428 practice, Springer, 95-101, 2013.
429 Ardizzone, F., Fiorucci, F., Mondini, A. C., and Guzzetti, F.: TXT-tool 1.039-1.1: Very-High Resolution Stereo
430 Satellite Images for Landslide Mapping, in: Landslide Dynamics: ISDR-ICL Landslide Interactive Teaching Tools
431 : Volume 1: Fundamentals, Mapping and Monitoring, edited by: Sassa, K., Guzzetti, F., Yamagishi, H., Arbanas,
432 Ž., Casagli, N., McSaveney, M., and Dang, K., Springer International Publishing, Cham, 83-94, 2018.
433 Brabb, E. E.: Innovative approaches to landslide hazard and risk mapping, International Landslide Symposium
434 Proceedings, Toronto, Canada, 1985, 17-22,
435 Cardinali, M., Ardizzone, F., Galli, M., Guzzetti, F., and Reichenbach, P.: Landslides triggered by rapid snow
436 melting: the December 1996–January 1997 event in Central Italy, Proceedings 1st Plinius Conference on
437 Mediterranean Storms, 2000, 439-448,
438 Carrara, A., Cardinali, M., Detti, R., Guzzetti, F., Pasqui, V., and Reichenbach, P.: GIS techniques and statistical
439 models in evaluating landslide hazard, Earth surface processes and landforms, 16, 427-445, 1991.
440 Costanzo, D., Rotigliano, E., Irigaray Fernández, C., Jiménez-Perálvarez, J. D., and Chacón Montero, J.: Factors
441 selection in landslide susceptibility modelling on large scale following the gis matrix method: application to the
442 river Beiro basin (Spain), 2012.
443 Diggle, P. J., Chetwynd, A. G., Häggkvist, R., and Morris, S. E.: Second-order analysis of space-time clustering,
444 Statistical methods in medical research, 4, 124-136, 1995.
445 Galli, M., Ardizzone, F., Cardinali, M., Guzzetti, F., and Reichenbach, P.: Comparing landslide inventory maps,
446 Geomorphology, 94, 268-289, 2008.
447 Gavin, D. G., Hu, F. S., Lertzman, K., and Corbett, P.: WEAK CLIMATIC CONTROL OF STAND-SCALE FIRE
448 HISTORY DURING THE LATE HOLOCENE, Ecology, 87, 1722-1732, 2006.
449 Gorum, T., Fan, X., van Westen, C. J., Huang, R. Q., Xu, Q., Tang, C., and Wang, G.: Distribution pattern of
450 earthquake-induced landslides triggered by the 12 May 2008 Wenchuan earthquake, Geomorphology, 133,
451 152-167, https://doi.org/10.1016/j.geomorph.2010.12.030, 2011.
452 Günther, A., Van Den Eeckhaut, M., Malet, J.-P., Reichenbach, P., and Hervás, J.: Climate-physiographically
453 differentiated Pan-European landslide susceptibility assessment using spatial multi-criteria evaluation and
454 transnational landslide information, Geomorphology, 224, 69-85,
455 https://doi.org/10.1016/j.geomorph.2014.07.011, 2014.
456 Guzzetti, F., Reichenbach, P., Cardinali, M., Galli, M., and Ardizzone, F.: Probabilistic landslide hazard
457 assessment at the basin scale, Geomorphology, 72, 272-299, 2005.
458 Guzzetti, F., Galli, M., Reichenbach, P., Ardizzone, F., and Cardinali, M.: Landslide hazard assessment in the
459 Collazzone area, Umbria, Central Italy, Natural Hazards and Earth System Science, 6, 115-131, 2006a.
460 Guzzetti, F., Reichenbach, P., Ardizzone, F., Cardinali, M., and Galli, M.: Estimating the quality of landslide
461 susceptibility models, Geomorphology, 81, 166-184, https://doi.org/10.1016/j.geomorph.2006.04.007, 2006b.
462 Guzzetti, F., Ardizzone, F., Cardinali, M., Rossi, M., and Valigi, D.: Landslide volumes and landslide mobilization
463 rates in Umbria, central Italy, Earth and Planetary Science Letters, 279, 222-229,
464 https://doi.org/10.1016/j.epsl.2009.01.005, 2009.
465 Guzzetti, F., Mondini, A. C., Cardinali, M., Fiorucci, F., Santangelo, M., and Chang, K.-T.: Landslide inventory
466 maps: New tools for an old problem, Earth-Science Reviews, 112, 42-66, 2012.
467 Haines, E.: Point in polygon strategies, Graphics gems IV, 994, 24-26, 1994.
468 Hinman, S. E., Blackburn, J. K., and Curtis, A.: Spatial and temporal structure of typhoid outbreaks in
469 Washington, DC, 1906–1909: evaluating local clustering with the G i* statistic, International Journal of Health
470 Geographics, 5, 13, 2006.
471 Jebur, M. N., Pradhan, B., and Tehrany, M. S.: Optimization of landslide conditioning factors using very high-
472 resolution airborne laser scanning (LiDAR) data at catchment scale, Remote Sensing of Environment, 152, 150-
473 165, 2014.
474 Keefer, D. K.: Statistical analysis of an earthquake-induced landslide distribution — the 1989 Loma Prieta,
475 California event, Engineering Geology, 58, 231-249, https://doi.org/10.1016/S0013-7952(00)00037-5, 2000.
476 Levine, N.: Crime mapping and the Crimestat program, Geographical analysis, 38, 41-56, 2006.
477 Lynch, H. J., and Moorcroft, P. R.: A spatiotemporal Ripley's K-function to analyze interactions between spruce
478 budworm and fire in British Columbia, Canada, Canadian Journal of Forest Research, 38, 3112-3119, 2008.
479 Mason, S. J., and Graham, N. E.: Areas beneath the relative operating characteristics (ROC) and relative
480 operating levels (ROL) curves: Statistical significance and interpretation, Quarterly Journal of the Royal
481 Meteorological Society, 128, 2145-2166, 2002.
482 Moore, I. D., and Wilson, J. P.: Length-slope factors for the Revised Universal Soil Loss Equation: Simplified
483 method of estimation, Journal of soil and water conservation, 47, 423-428, 1992.

Natural Hazards
and Earth System
Sciences
Open Access
Discussions
EGU

484 Moore, I. D., Gessler, P., Nielsen, G., and Peterson, G.: Soil attribute prediction using terrain analysis, Soil
485 Science Society of America Journal, 57, 443-452, 1993.
486 Neuhäuser, B., Damm, B., and Terhorst, B.: GIS-based assessment of landslide susceptibility on the base of the
487 weights-of-evidence model, Landslides, 9, 511-528, 2012.
488 Phillips, J.: Evolutionary geomorphology: thresholds and nonlinearity in landform response to environmental
489 change, 2006.
490 Reichenbach, P., Rossi, M., Malamud, B. D., Mihir, M., and Guzzetti, F.: A review of statistically-based landslide
491 susceptibility models, Earth-Science Reviews, 180, 60-91, https://doi.org/10.1016/j.earscirev.2018.03.001,
492 2018.
493 Riley, S. J., DeGloria, S., and Elliot, R.: Index that quantifies topographic heterogeneity, intermountain Journal
494 of sciences, 5, 23-27, 1999.
495 Ripley, B. D.: The second-order analysis of stationary point processes, Journal of applied probability, 13, 255-
496 266, 1976.
497 Ripley, B. D.: Modelling spatial patterns, Journal of the Royal Statistical Society. Series B (Methodological),
498 172-212, 1977.
499 Rossi, M., Guzzetti, F., Reichenbach, P., Mondini, A. C., and Peruccacci, S.: Optimal landslide susceptibility
500 zonation based on multiple forecasts, Geomorphology, 114, 129-142,
501 https://doi.org/10.1016/j.geomorph.2009.06.020, 2010.
502 Samia, J., Temme, A., Bregt, A., Wallinga, J., Guzzetti, F., Ardizzone, F., and Rossi, M.: Do landslides follow
503 landslides? Insights in path dependency from a multi-temporal landslide inventory, Landslides, 14, 547-558,
504 10.1007/s10346-016-0739-x, 2017a.
505 Samia, J., Temme, A., Bregt, A., Wallinga, J., Guzzetti, F., Ardizzone, F., and Rossi, M.: Characterization and
506 quantification of path dependency in landslide susceptibility, Geomorphology, 292, 16-24,
507 https://doi.org/10.1016/j.geomorph.2017.04.039, 2017b.
508 Samia, J., Temme, A., Bregt, A. K., Wallinga, J., Stuiver, J., Guzzetti, F., Ardizzone, F., and Rossi, M.:
509 Implementing landslide path dependency in landslide susceptibility modelling, Landslides, 1-16, 2018.
510 Sato, H. P., Hasegawa, H., Fujiwara, S., Tobita, M., Koarai, M., Une, H., and Iwahashi, J.: Interpretation of
511 landslide distribution triggered by the 2005 Northern Pakistan earthquake using SPOT 5 imagery, Landslides, 4,
512 113-122, 10.1007/s10346-006-0069-5, 2007.
513 Schlögel, R., Torgoev, I., De Marneffe, C., and Havenith, H. B.: Evidence of a changing size–frequency
514 distribution of landslides in the Kyrgyz Tien Shan, Central Asia, Earth Surface Processes and Landforms, 36,
515 1658-1669, 2011.
516 Smith, T.: Notebook on spatial data analysis, Lecture Note, 2016.
517 Tonini, M., Pedrazzini, A., Penna, I., and Jaboyedoff, M.: Spatial pattern of landslides in Swiss Rhone Valley,
518 Natural Hazards, 73, 97-110, 2014.
519 Van Westen, C., Rengers, N., and Soeters, R.: Use of geomorphological information in indirect landslide
520 susceptibility assessment, Natural hazards, 30, 399-419, 2003.
521 Van Westen, C. J., Castellanos, E., and Kuriakose, S. L.: Spatial data for landslide susceptibility, hazard, and
522 vulnerability assessment: an overview, Engineering geology, 102, 112-131, 2008.
523 Varnes, D. J.: Landslide hazard zonation: a review of principles and practice, 1984.
524 Ye, X., Xu, X., Lee, J., Zhu, X., and Wu, L.: Space–time interaction of residential burglaries in Wuhan, China,
525 Applied Geography, 60, 210-216, https://doi.org/10.1016/j.apgeog.2014.11.022, 2015.

526